Analysis of effect of tool geometry on plastic flow during friction stir spot welding using particle method

Hirasawa, Shigeki
Harsha, Badarinarayan
Okamoto, Kazutaka
Tomimura, Toshio
Kawanami, Tsuyoshi

(Citation)
Journal of Materials Processing Technology,210(11):1455-1463

(Issue Date)
2010-08

(Resource Type)
journal article

(Version)
Accepted Manuscript

(URL)
https://hdl.handle.net/20.500.14094/90002185

Analysis of Effect of Tool Geometry on Plastic Flow during Friction Stir Spot Welding using Particle Method

Shigeki Hirasawa[1], Harsha Badarinarayan[2], Kazutaka Okamoto[3],
Toshio Tomimura[4], and Tsuyoshi Kawanami[1]

ABSTRACT

The effect of tool geometry on the plastic flow and material mixing during friction stir spot welding (FSSW) is investigated using the particle method approach. For spot welds made with a cylindrical pin tool with flat shoulder, the model predicts the material flow at the pin periphery to be in the upward direction and the material is pushed downward beneath the shoulder giving rise to the resultant hook geometry. Other pin geometries evaluated include tapered pin, inverse tapered pin, triangular pin, convex shoulder, and concave shoulder. With good correlation with experimental trials, this model is then used to predict the material flow for spot welds. The material flow, and thereby the resultant hook formation, is quantified using numerical methods and is expressed as standard deviation of the particle movement. A triangular pin with a concave shoulder is the preferred tool geometry from the current study that results in high strength spot welds.

Key words: Friction Stir Spot Welding; Manufacturing Process Simulation; Temperature Distribution; Plastic Deformation; Particle Method

1. INTRODUCTION

Friction stir welding is a relatively new solid state joining process. A non-consumable rotating tool is plunged in a controlled fashion into the workpieces that are being joined. Frictional heat is generated at the tool-work material interface by the tool under the action of a vertical load, thereby reducing the material flow stress. The tool is then traversed along the desired weld path at a predetermined speed to realize the weld. The localized heating softens material around the tool and the action of tool rotation combined with translation results in a solid state joint being produced. The main advantage of the friction stir welding is that the temperature during welding is less than the melting temperature of the workpieces, thus the deformation is significantly less than conventional arc welding technique. Friction stir spot welding (FSSW) is a variant of the friction stir welding and is schematically illustrated in Fig. 1. A non-consumable rotating tool is plunged into the workpieces to be joined. Upon reaching the desired plunge depth, the rotating tool is held in that position for a pre-determined finite time (sometimes referred to as dwell period). Subsequent to that, the rotating tool is then retracted from the welded joint leaving behind a friction stir spot weld. FSSW can be considered as a transient process due to its short cycle time (usually a few seconds). During FSSW, tool penetration and the dwell period essentially determine the heat generation, material plasticization around the pin, weld geometry and therefore mechanical properties of the welded joint. The tool has two distinct parts - the shoulder and the pin. The shoulder generates bulk of the frictional or deformational heat. The pin assists in material flow between the workpieces. Features are incorporated on the shoulder and pin surfaces to further aid these functionalities. If process conditions for the welds are not optimized, the resulting joint may contain weld defects. Presently, optimum welding conditions are determined in many experiments and a numerical simulation code to calculate optimum welding conditions is desired.

Many investigators have tried to simulate friction stir welding process. Langerman et al. (2003), and Colegrove et al. (2004) analyzed the temperature distribution and the flow of metals by using the computational fluid dynamic code FLUENT with non-Newtonian fluid model. Dörfler (2008) analyzed the metal flow during the welding of different materials by using the computational fluid dynamic code COMSOL with the level set method. When the fluid model is used, it is difficult to approximate metal properties of the plastic deformation behavior. Khandkar et al. (2003), McCune et al. (2004), Schmidt et al. (2005), Zhang et al. (2008, 2009), and Rajamanickam et al. (2009) analyzed the temperature distribution and the plastic deformation by using the finite element code ABAQUS with an elastic-plastic deformation model. It is necessary to analyze the plastic deformation with very high strain rates. Schmidt et al. (2005) analyzed the void formation in metal at non-successful condition. Zahedul et al. (2006) analyzed the residual thermal stresses in welded metals. The present authors (2005, 2006, 2009)

analyzed the temperature distribution by the finite element method, and also analyzed the plastic flow of material by the particle method during friction stir welding process. The particle method is preferable to analyze large plastic deformation behavior with very high strain rates. Badarinarayan et al. (2007, 2009a, 2009b) reported experimental results of the temperature distribution, the flow pattern and the effect of tool geometry on metallurgical bond for FSSW.

In the work reported here, the temperature distribution and the plastic flow of material are analyzed during FSSW process. The plastic flow is analyzed with the elastic-plastic deformation model using the particle method. Numerical analysis aids in understanding the effect of different tool geometries on the material flow during FSSW. The outcome of this research will help in determining the optimum tool geometry for this process.

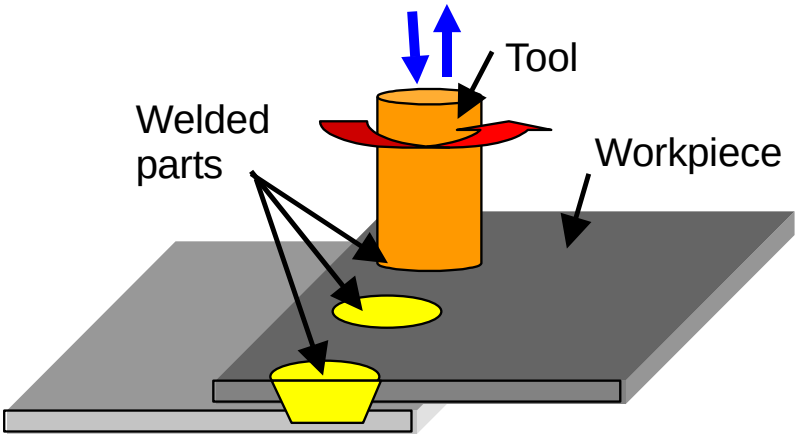

(a) Isometric view

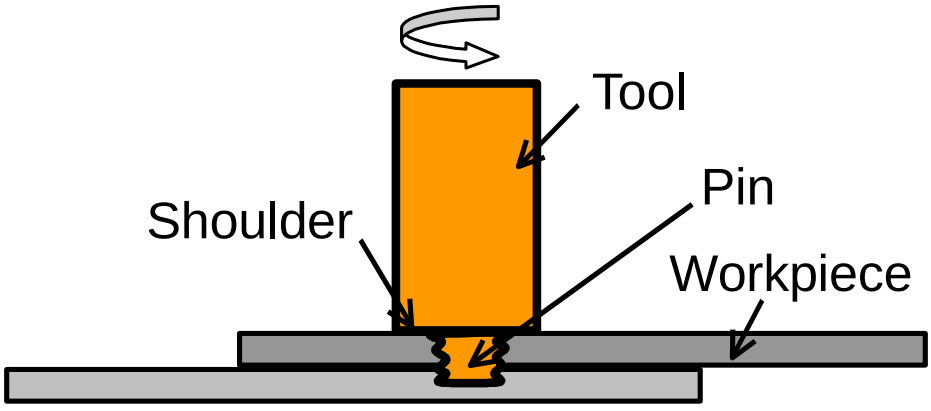

(b) Vertical cross section

Fig. 1 Schematic view of friction stir spot welding (FSSW)

2. ANALYTICAL METHOD

A two-step approach is undertaken in the current numerical analysis. First, the temperature distribution is computed at a given condition (of tool geometry, plunge force and material flow velocity). Then, using this temperature distribution, the plastic flow of material is analyzed.

In order to simplify the modeling, the welding was done on a single sheet and hence called as 'Spot-on-Plate' type welding. The thickness of the workpiece is 2.5 mm. The FSSW tool has a shoulder diameter of 12mm, cylindrical pin diameter of 5 mm and pin length of 1.25 mm. The shoulder profile is flat. In addition to this, other pin geometries evaluated were: triangular pin, tapered pin, inverse tapered pin. Also, concave and convex shoulder profiles were also modeled. The process conditions used for welding were: tool rotational speed 1500 rpm, plunge rate 3.3 mm/s for 0.44 s. The calculation conditions for the numerical model of temperature distribution are shown in Fig. 2. The dimension of the workpiece considered is 100 mm × 100 mm × 2.5 mm. There is 0.1 mm air gap between the workpiece and the anvil.

Temperature distribution is calculated with the unsteady thermal conduction equation.

$$\rho c\left(\frac{\partial T}{\partial t}+u\frac{\partial T}{\partial x}+v\frac{\partial T}{\partial y}+w\frac{\partial T}{\partial z}\right)=\lambda\left(\frac{\partial^2 T}{\partial x^2}+\frac{\partial^2 T}{\partial y^2}+\frac{\partial^2 T}{\partial z^2}\right)+q \tag{1}$$

where, x, y, and z are the coordinates (m), t is the time (s), u, v, and w are the flow velocity (m/s), T is temperature (°C), ρ is density (kg/m^3), c is specific heat (J/(kg K)), λ is thermal conductivity (W/(m K)), and q is heat generation rate per unit volume (W/m^3). Heat is assumed to be generated at the contact surface between the tool and the workpiece. It has been reported that the effect of the location of heat generation region on temperature distribution near the tool is not significant (Hirasawa et al., 2005). Local contact surface heat generating rate q_0 (W/m^2) is calculated by Eq. (2).

$$q_0 = \pi d\mu pN \tag{2}$$

where, d is diameter (m), μ is the dynamic friction coefficient (μ = 0.6 in this work (Tomimura et al., 2006)), p is contact pressure (Pa), and N is rotating speed (N = (1500/60) round/s). Plunge force of the tool is assumed to be constant 1400 N, which was obtained from experimental data (Badarinarayan et al., 2007), and the contact pressure p is calculated from the plunge force. The initial temperature of the workpiece is 25°C. Boundary conditions for temperature analysis are as following. The temperature of the periphery of the workpiece, and top end of the tool are fixed to be 25°C. Also, the temperature of

the anvil is fixed to be 25°C. Other boundary conditions are adiabatic. The thermal conduction in the air gap between the workpiece and the anvil is computed. The workpiece is aluminum alloy A6061 with thermal conductivity 180 W/(m K), density 2700 kg/m^3 and specific heat 896 J/(kg K). Equation (1) is calculated using the finite element method. The temperature change is calculated with the time step of 0.044 s until the final time of 0.44 s.

The plastic flow of material is analyzed with the obtained temperature distribution. The calculation region of plastic flow in the workpiece is assumed to be 18 mm in diameter. The calculation region of the plastic flow is smaller than that of the temperature distribution shown in Fig. 2, because the plastic flow region is smaller then the temperature diffusion region. The plastic flow is calculated with the elastic-plastic deformation equations shown in Eqs. (3) and (4).

$$\rho \frac{\partial^2 r_\alpha}{\partial t^2} = \frac{\partial}{\partial x_\beta}\left(\frac{\nu E}{(1+\nu)(1-2\nu)} \varepsilon_{\gamma\gamma} \delta_{\alpha\beta} + \frac{E}{(1+\nu)} \varepsilon_{\alpha\beta} \right) + K_\alpha \tag{3}$$

$$\varepsilon_{\alpha\beta} = \frac{1}{2}\left(\frac{\partial u_\alpha}{\partial x_\beta} + \frac{\partial u_\beta}{\partial x_\alpha} \right) \tag{4}$$

where, r_α is the coordinates of the material (m), t is the time (s), x_β is the space coordinates in Cartesian system (m), ρ is the density (kg/m^3), E is the Young's modulus (Pa), ν is the Poisson ratio, $\varepsilon_{\alpha\beta}$ is the strain tensor, $\delta_{\gamma\gamma}$ is the Kronecker delta, K_α is the external body force (N/m^3), and u_α is the deformation vector (m). The elastic-plastic deformation equations are analyzed using the particle method. In the particle method, the workpiece material is assumed to be composed of several 'particles', as shown in Fig. 3, and the movements of these particles are computed. When the material is expressed with many particles, the deformation vector u_{ij} is calculated by Eq. (5).

$$u_{ij} = \left(r_j - r_i\right) - R\left(r^0{}_j - r^0{}_i\right) \tag{5}$$

where, r_i is the coordinates of the particle (m), R is the rotation matrix, and suffix 0 is the initial condition. Normal stress $\sigma^n{}_{ij}$, and shear stress $\sigma^s{}_{ij}$ is obtained by Eqs. (6) and (7).

$$\sigma^n{}_{ij} = \frac{E}{(1+\nu)} \varepsilon^n{}_{ij} \tag{6}$$

$$\sigma^{s}{}_{ij} = \frac{E}{(1+\nu)}\varepsilon^{s}{}_{ij} \tag{7}$$

Plastic deformation is assumed to occur when the maximum tensile stress exceeds the yield stress. These equations are analyzed by the particle method with the moving-particle semi-implicit method (Chikazawa et al., 2001; Kondo et al, 2006). The particle method is a meshless method. In the particle method, the workpiece material is assumed to be composed of several 'particles', as shown in Fig. 3, and the movement of these particles are computed. These particles are essential spring models as shown in Fig. 4. These particles are interconnected in the normal direction and the tangential direction.

Figure 3 shows the initial condition of particles in vertical cross section. The workpiece is comprised of 53000 particles with a pitch of 0.25 mm. Red particles are in the plastic flow region. Blue particles are those on the tool or those that represent fixed position regions. Black particles show the horizontal position at 1 mm from the upper surface, which will be compared with contact surface of overlapped two workpieces in experiment. In the calculation, the position of the moving tool is given at each time step. The positions of the anvil and the periphery of the workpiece are fixed. Slip at the contact surfaces between the tool and the workpiece is neglected. The workpiece is aluminum alloy A6061 with the Young's modulus 65 GPa, and the Poisson ratio 0.3. The yield stress is a function of the local temperature as shown in Fig. 5 (Chao et al., 1998). Movement of particles is calculated with the time step of 0.00002 s until the final time of 0.44 s. The computation time is shortened by using the table-look-up procedure (Aratani, 1995).

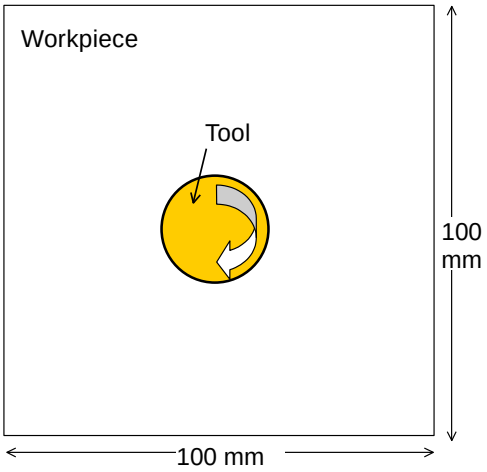

(a) Top view

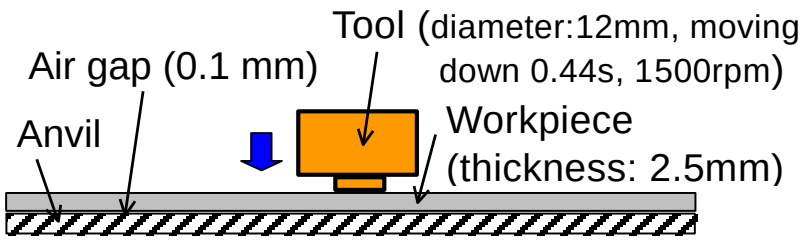

(b) Vertical cross section

Fig. 2 Calculation model of temperature distribution

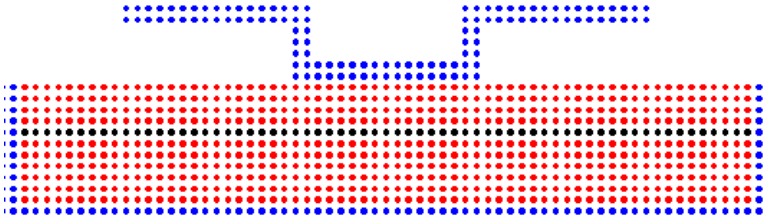

Fig. 3 Initial condition of particles in vertical cross section

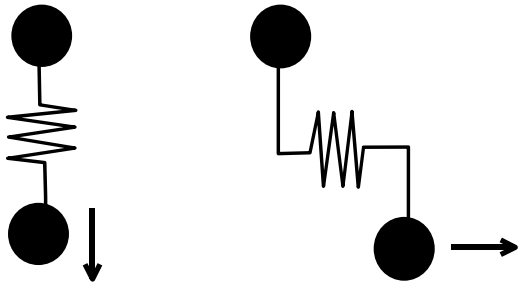

(a) Normal direction **(b) Tangential direction**

Fig. 4 Spring model

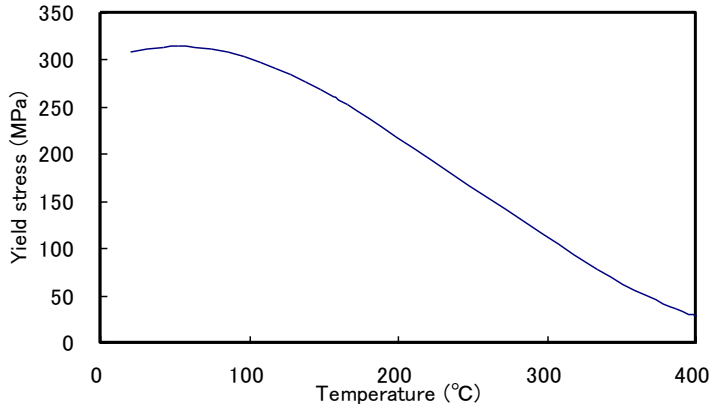

Fig. 5 Yield stress of workpiece

3. CALCULATION RESULTS

3.1 Standard Cylindrical Pin

The standard cylindrical pin of the tool is 5 mm in diameter and 1.25mm in length. The shoulder diameter of the tool is 12mm. Figure 6 shows the calculation result of temperature distributions in the workpiece at time 0.44 s for a standard cylindrical pin. Temperature distribution is axisymmetric and the temperature below the rotation tool is 340°C at 0.44 s. Heat transfer phenomena in FSSW is axisymmetric. Material flow caused by the tool rotation is nearly circular, and the effect of the circular flow velocity on the axisymmetric temperature distribution is small. Figure 7 shows the calculated workpiece temperature profile just below the tool and at a distance of 2.5 mm (near the pin circumference), 6 mm (near the shoulder circumference), and 8 mm from the tool axis. There is a slight drop in temperature below the shoulder surface at 0.35 s, this is because the shoulder comes in contact with the workpiece and hence the local pressure decreases to about one-seventh of its original value in that region for a constant plunge force of the tool. However, the thermal conduction heat flux in the workpiece is almost same at that instant. This drop in temperature is not observed outside the region of the shoulder diameter. Temperature below the tool should be high enough to soften the workpiece but less than the melting temperature. Plastic flow and mixing of material are analyzed using the obtained temperature distribution.

Figure 8 shows the instantaneous snap-shot of the material flow at different time instances during the tool plunging phase. The black particles are an indication of the original particle position that was 1 mm from the upper surface of the workpiece, as shown in Fig. 3. The material flow shows particle velocity vectors. The model predicts the material flow at the pin periphery is in the upward direction. Near the shoulder, there are two flow patterns observed – beneath the shoulder, the material is pushed downward due to the force acting from the shoulder face, whereas on the shoulder periphery the material flows

upward and outward due to extrusion of the material that is caused by the shoulder plunge. This extruded material shows up on the specimen surface as burr. The material flow is similar to that observed in experimental trial shown in Fig. 9 (Badarinarayan et al., 2007). Thus, this modeling technique gives a visual of the complex material mixing phenomena during FSSW.

Figure 10 shows the numerical results of the average position of particles shown in black particles in Fig. 8 (d) (that were originally at 1 mm from the upper surface of the workpiece), and it corresponds to the contact surface of overlapped two workpieces. The average position has a round upward bending (called as 'hook'). Partial metallurgical bond observed in the weld region between the overlapped metal sheets in experimental (Badarinarayan et al., 2009a). The numerical result shown in Fig. 10 explicitly shows this resulting hook geometry which closely matches the experimental result.

Figure 11 shows the standard deviation of movement of these black particles at time 0.44 s. The standard deviation of the movement signifies material mixing. The mixing is large near the periphery of the pin.

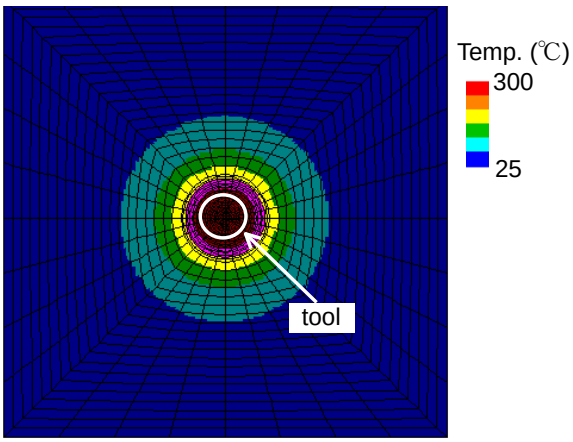

Fig. 6 Temperature distribution of workpiece at 0.44 s for cylindrical pin

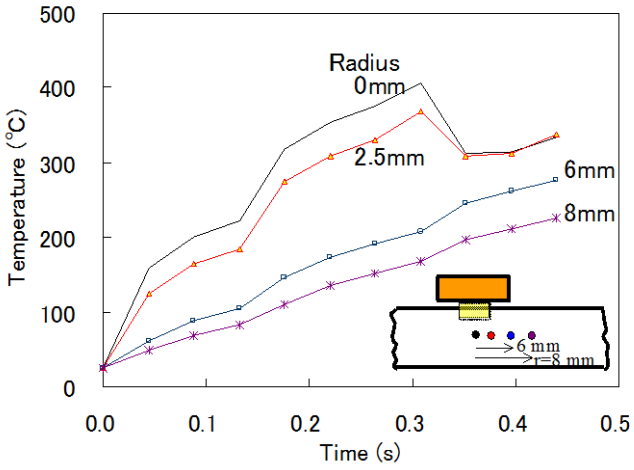

Fig. 7 Temperature change of workpiece for cylindrical pin

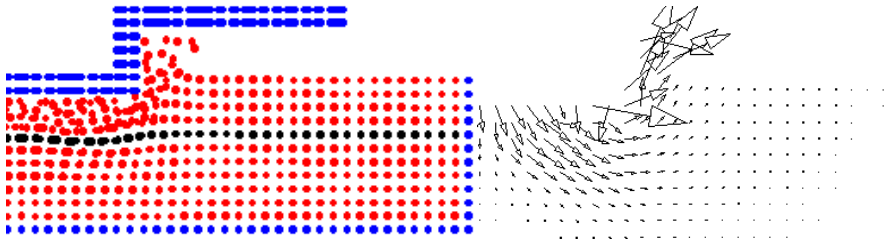

(a) 0.13 s

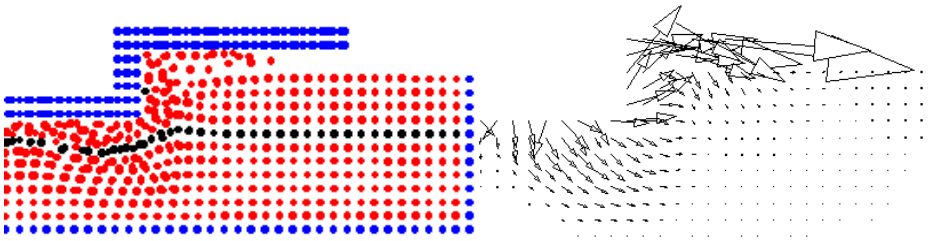

(b) 0.26 s

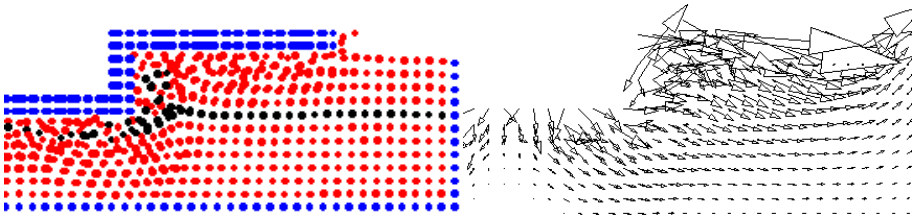

(c) 0.35 s

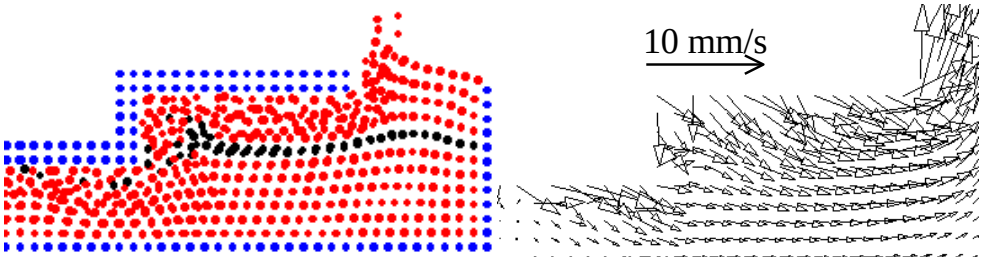

(d) 0.44 s

Fig. 8 Change of positions of particles (left) and flow pattern (right) for cylindrical pin

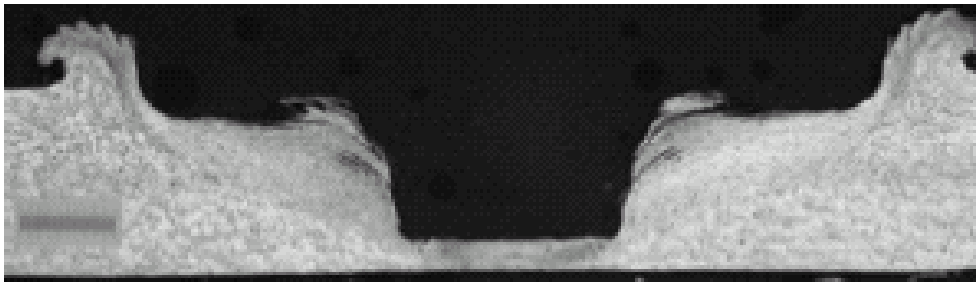

Fig. 9 Vertical cross section of FSSW weld specimen for cylindrical pin (Badarinarayan et al., 2007)

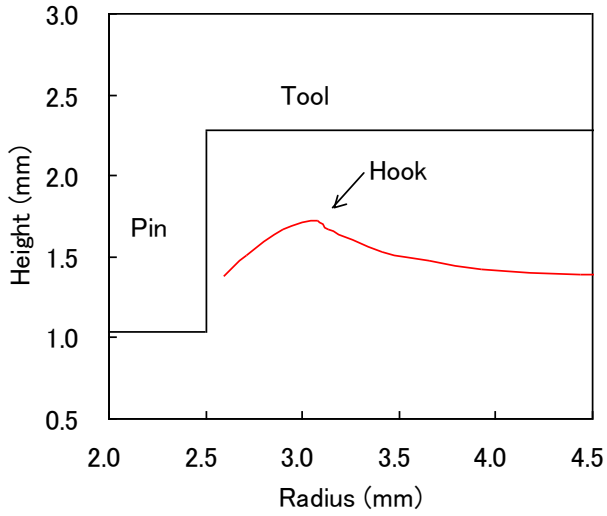

Fig. 10 Average position of particles that were originally at 1 mm from upper surface of workpiece at 0.44 s for cylindrical pin

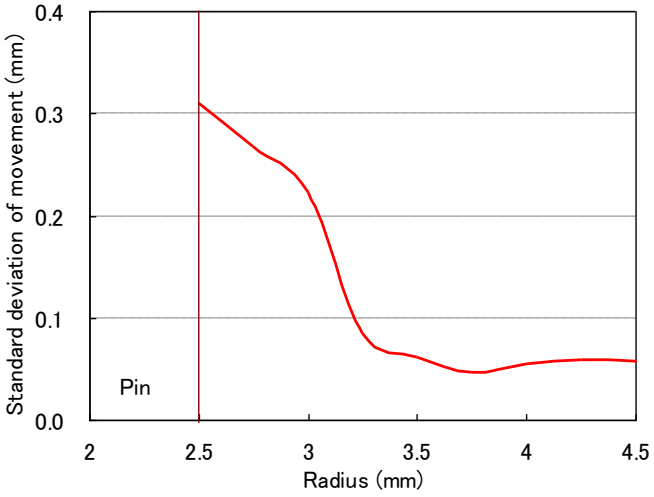

Fig. 11 Standard deviation of movement of particles at 0.44 s for cylindrical pin

3.2 Tapered Pin

Plastic flow of material is calculated for a tool with tapered pin (Fig. 12). The pin diameter at the root of the pin is 5 mm whereas at the free end it is 4 mm. Pin length is 1.25 mm.

Figure 13 shows the calculation result of the positions of particles at 0.44 s. Figure 14 shows total material flow pattern from 0 s to 0.44 s. The flow is along the tapered surface of the pin. Figure 15 shows the average position of particles (that were originally at 1 mm from the upper surface of the workpiece) at time 0.44 s. The 'hook' formation is smaller than that for the standard cylindrical pin (Fig. 10). The standard deviation of these particles at time 0.44 s is similar to that of the standard cylindrical pin (Fig. 11).

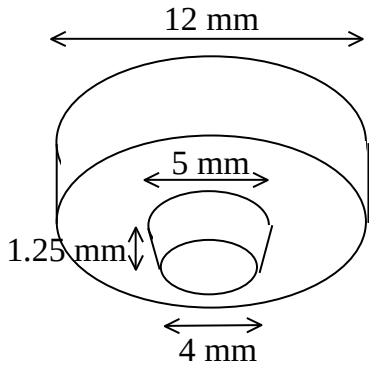

Fig. 12 Tapered pin tool geometry

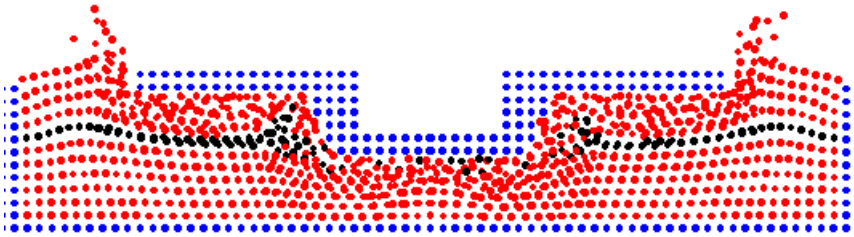

Fig. 13 Vertical positions of particles at 0.44 s for tapered pin

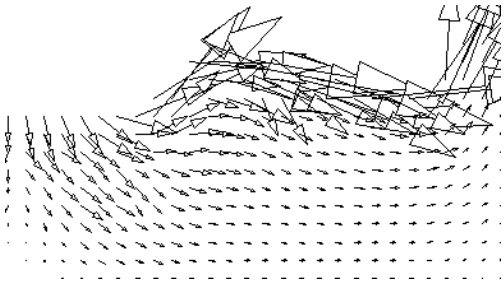

Fig. 14 Total flow pattern from 0 s to 0.44 s for tapered pin

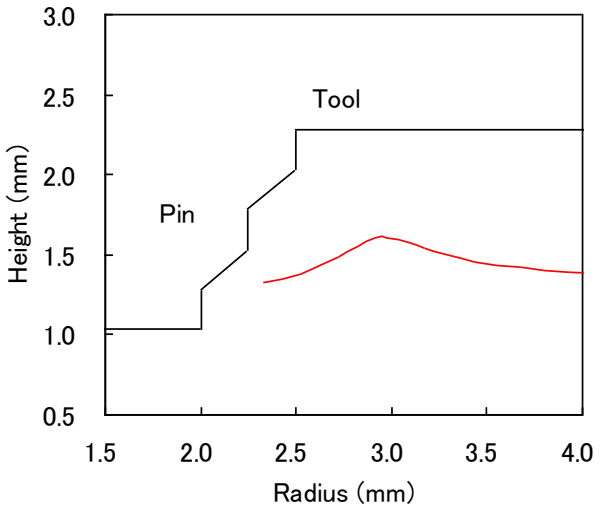

Fig. 15 Average position of particles that were originally at 1 mm from upper surface of workpiece at 0.44 s for tapered pin

3.3 Inverse Tapered Pin

Plastic flow of material is calculated for a tool with inverse tapered pin (Fig. 16). The pin diameter at the root of the pin is 5 mm whereas at the free end it is 6 mm. Pin length is 1.25 mm.

Figure 17 shows the calculation result of the positions of particles at 0.44 s after plunge. Figure 18 shows total material flow pattern from 0 s to 0.44 s. Figure 19 shows the average position of particles (that were originally at 1 mm from the upper surface of the workpiece) at time 0.44 s. The 'hook' formation is similar to that for the standard cylindrical pin. The standard deviation of these particles at time 0.44 s is similar to that of the standard cylindrical pin (Fig. 11).

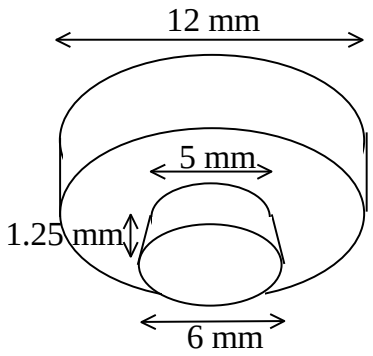

Fig. 16 Inverse tapered pin tool geometry

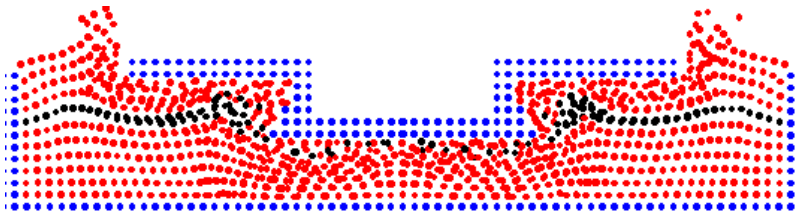

Fig. 17 Vertical positions of particles at 0.44 s after plunge for inverse tapered pin

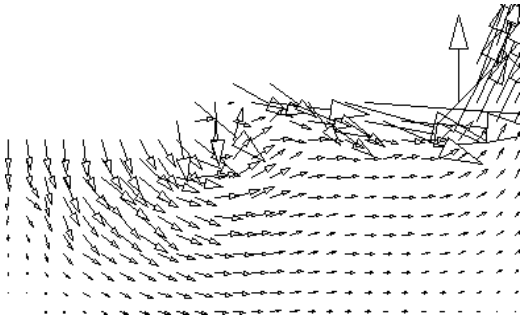

Fig. 18 Total flow pattern from 0 s to 0.44 s for inverse tapered pin

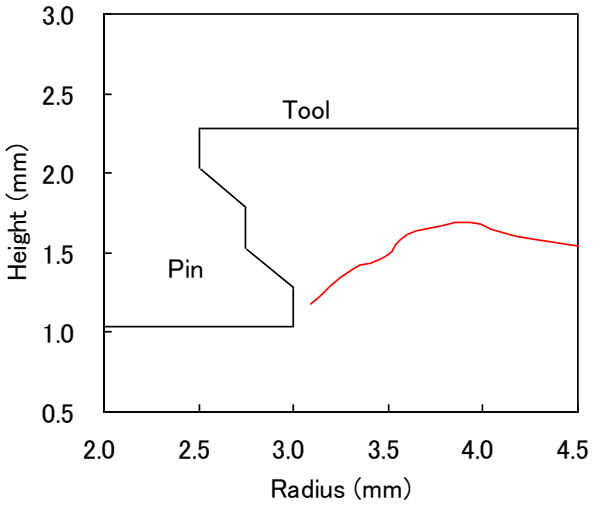

Fig. 19 Average position of particles that were originally at 1 mm from upper surface of workpiece at 0.44 s for inverse tapered pin

3.4 Convex Shoulder

Plastic flow of material is calculated for a tool with convex shoulder (Fig. 20). The length of the convex shoulder is 0.5 mm (inclined angle of the face is 10°), the diameter of cylindrical pin is 5 mm, and the pin length is 0.75 mm.

Figure 21 shows the calculation result of the positions of particles at 0.44 s after plunge. Figure 22 shows total material flow pattern from 0 s to 0.44 s. Figure 23 shows the average position of particles (that were originally at 1 mm from the upper surface of the workpiece) at time 0.44 s. There is no 'hook' formation in the weld region generated due to this tool geometry. Figure 24 shows the standard deviation of these particles at time 0.44 s. This magnitude is quite small indicating that the resultant material mixing is poor. Therefore the strength of these spot welds is expected to be lower than those made with standard cylindrical pin.

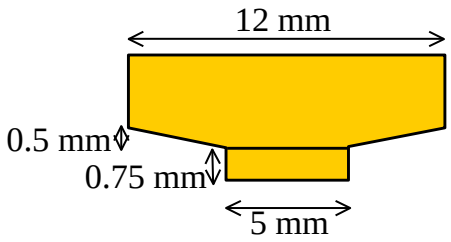

Fig. 20 Convex shoulder tool geometry

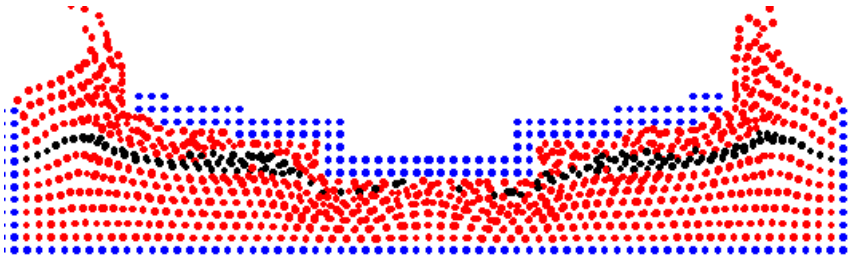

Fig. 21 Vertical positions of particles at 0.44 s after plunge for convex shoulder

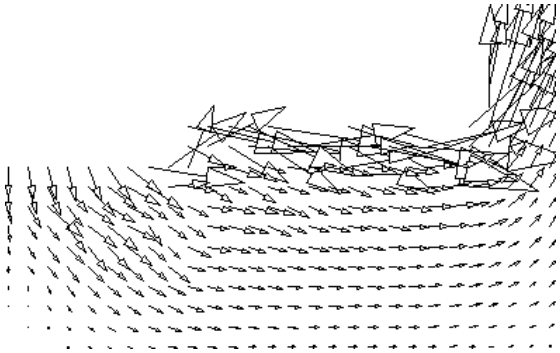

Fig. 22 Total flow pattern from 0 s to 0.44 s for convex shoulder

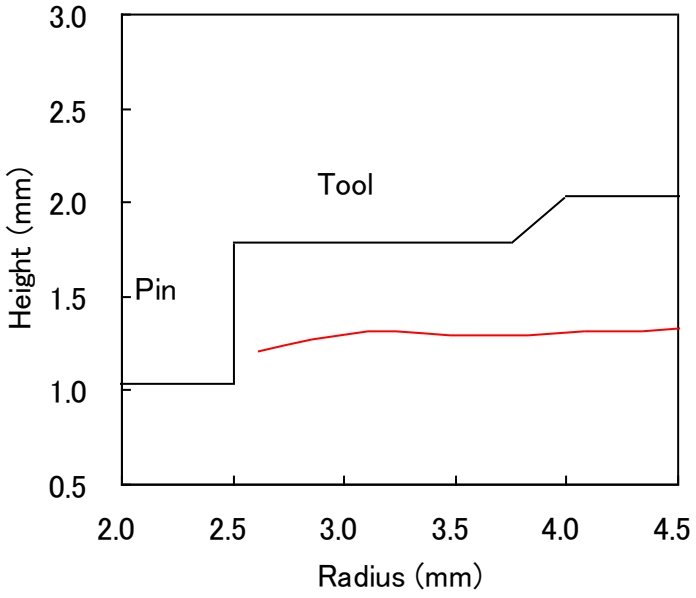

Fig. 23 Average position of particles that were originally at 1 mm from upper surface of workpiece at 0.44 s for convex shoulder

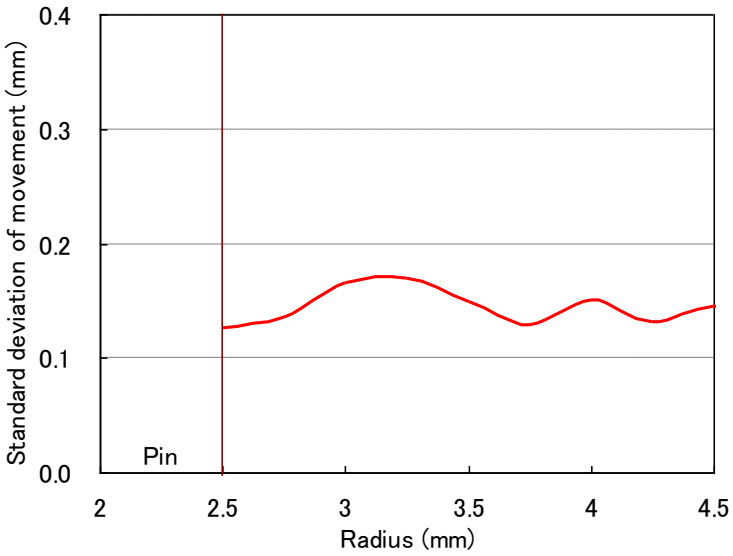

Fig. 24 Standard deviation of movement of particles at 0.44 s for convex shoulder

3.5 Concave Shoulder

Plastic flow of material is calculated for a tool with concave shoulder (Fig. 25). The length of the concave shoulder is 0.5 mm (inclined angle of the face is 10°), the diameter of cylindrical pin is 5 mm, and the pin length is 1.75 mm.

Figure 26 shows the calculation result of the positions of particles at 0.44 s after plunge. Figure 27 shows positions of particles and material flow pattern at 0.35 s during the tool plunging phase. Upward material flow at the pin periphery and downward flow beneath the shoulder are stronger than the standard cylindrical pin (Fig. 8). Figure 28 shows the average position of particles (that were originally at 1 mm from the upper surface of the workpiece) at time 0.44 s. There is a sharp 'hook' formation observed. The sharp 'hook' formation prevents failure propagation along the contact surface of overlapped two workpieces and increases welding strength (Badarinarayan et al., 2009a). Figure 29 shows the standard deviation of the particles (that were originally at 1 mm from the upper surface of the workpiece) at time 0.44 s. The magnitude of standard deviation is smaller than that predicted for the standard cylindrical pin indicating that less mixing. Tool shoulder profile has a significant influence on the material mixing and eventually the static strength.

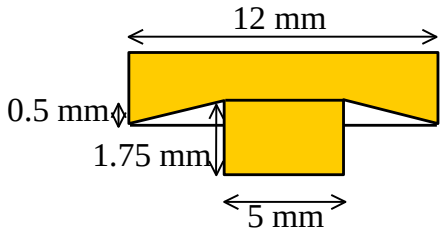

Fig. 25 Concave shoulder tool geometry

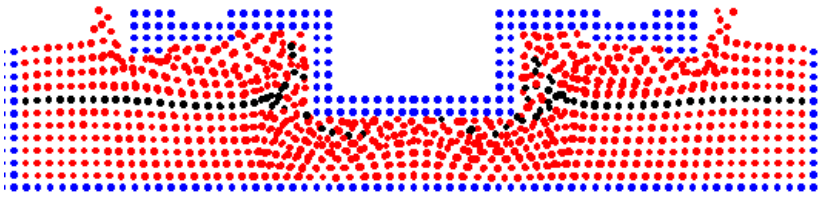

Fig. 26 Vertical positions of particles at 0.44 s after plunge for concave shoulder

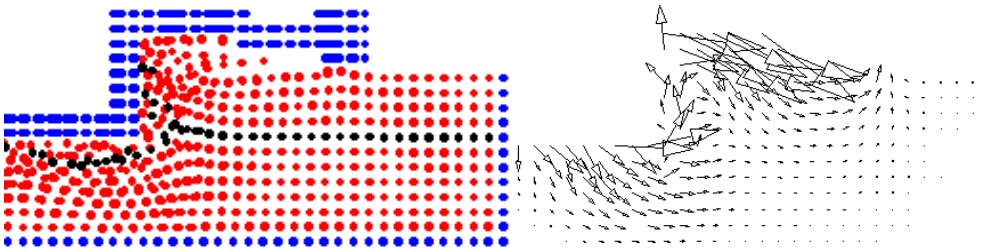

Fig. 27 Positions of particles (left) and flow pattern (right) at 0.35 s for concave shoulder

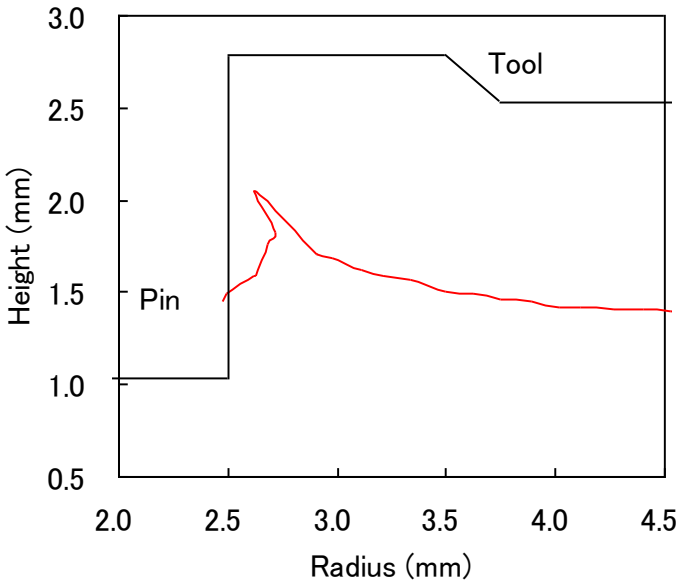

Fig. 28 Average position of particles that were originally at 1 mm from upper surface of workpiece at 0.44 s for concave shoulder

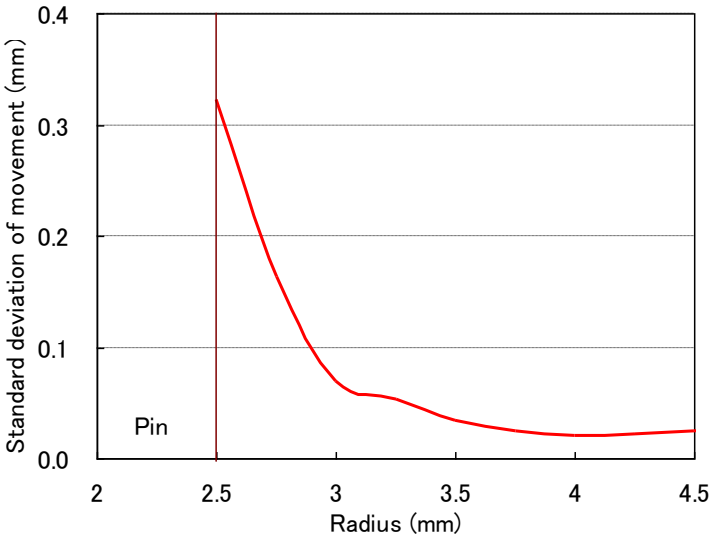

Fig. 29 Standard deviation of movement of particles at 0.44 s for concave shoulder

3.6 Triangular Pin with Concave Shoulder

Figure 30 shows the schematic illustration of the triangular pin geometry. The circumscribed pin diameter is 5mm. The tool has a concave shoulder with a 10° angle of concavity. Figure 31 shows the calculation result of temperature changes of the workpiece just below the tool and at a distance of 2.5, 6, and 8 mm from the tool axis. There is more heat generation by plastic deformation near the triangular pin and temperature is larger than that of the cylindrical pin (Fig. 7).

Figure 32 shows the calculation result of the particle positions in the vertical cross section at 0.44 s. Figure 33 shows the calculation result of the particle positions in the horizontal cross section and material flow pattern in the vertical cross section at time 0.429 and 0.436 s. The horizontal particle positions are shown at the tip of the pin. At the corner of the triangular pin (Fig. 33 (b)), the flow is the outside and downward direction. At the cut portion between the corners of the triangular pin (Fig. 33 (a)), the flow is the inside and upward direction. Figure 34 shows the material flow pattern in the horizontal cross section at 0.436 s. At the corner of the triangular pin (marked as 'A' in Fig. 34), the flow is in the outward direction. At the advancing side of the corner of the triangular pin (marked as 'B'), the flow is along the direction of rotation. At the backside of the corner of the triangular pin (marked as 'C'), the flow is the inward direction. This flow pattern enhances the mixing of metal material.

Figure 35 shows the average position of particles (that were originally at 1 mm from the upper surface of the workpiece) at time 0.44 s. There is a sharp 'hook' formation near the pin. Figure 36 shows the standard deviation of movement of particles at the contact surface at time 0.44 s. This results shows that the mixing around the pin is greatly enchanced. The strong material flow and mixing occur at the corner of the triangular pin. Figure 37 shows vertical cross section of experiment result for a triangular pin (Badarinarayan et al., 2009a), showing the suppressed hook geometry. Badarinarayan et al. (2009b) reported the weld strength for a tool with triangular pin with concave shoulder is stronger than that for the standard cylindrical pin. Experimental results showed that welds made with the cylindrical pin have a continuous hook which bypasses the stir zone and terminates close to the keyhole. By contrast, for welds made with the triangular pin, the hook is directed upwards and then arrested at the periphery of the stir zone. The difference in the hook shape can be attributed to the material flow. The calculation results presented here is in line with experimental trials. A triangular pin with a concave shoulder is preferred for friction stir spot welding as this configuration results in welds with a suppressed hook geometry yielding high strength welds.

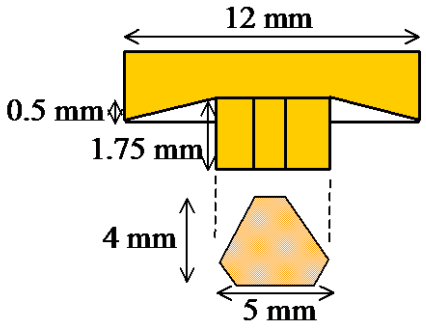

Fig. 30 Tool geometry of triangular pin with concave shoulder

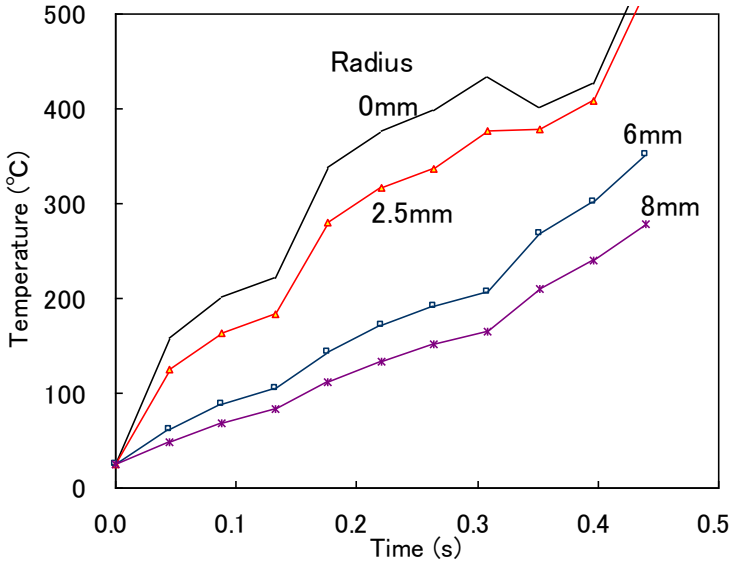

Fig. 31 Temperature change of workpiece for triangular pin

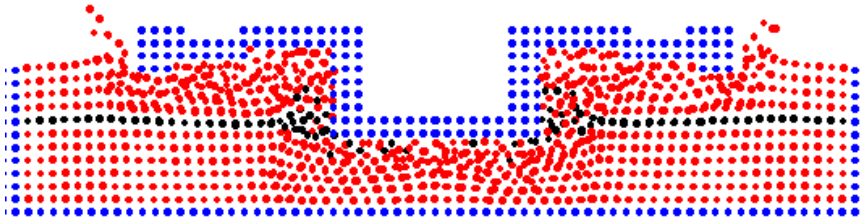

Fig. 32 Vertical positions of particles at 0.44 s for triangular pin with concave shoulder

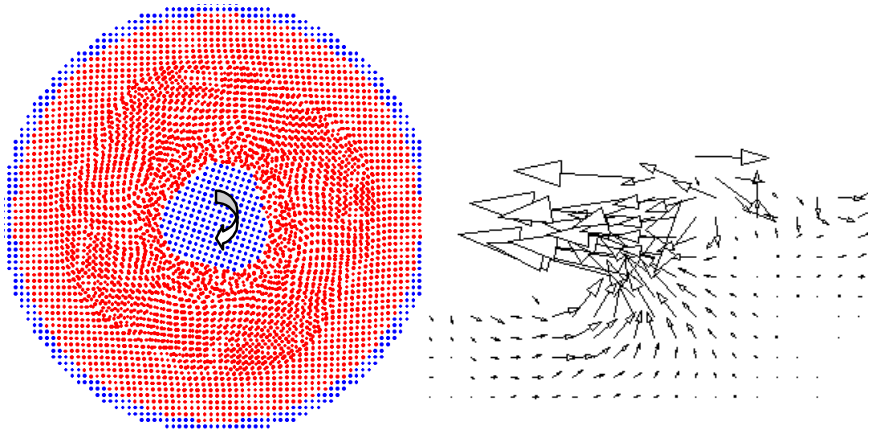

(a) 0.429 s

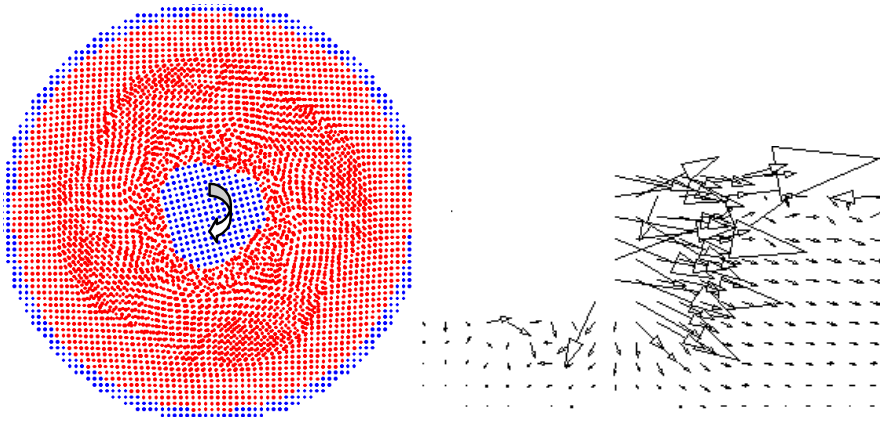

(b) 0.436 s

Fig. 33 Change of horizontal positions of particles (left) and flow pattern (right) for triangular pin

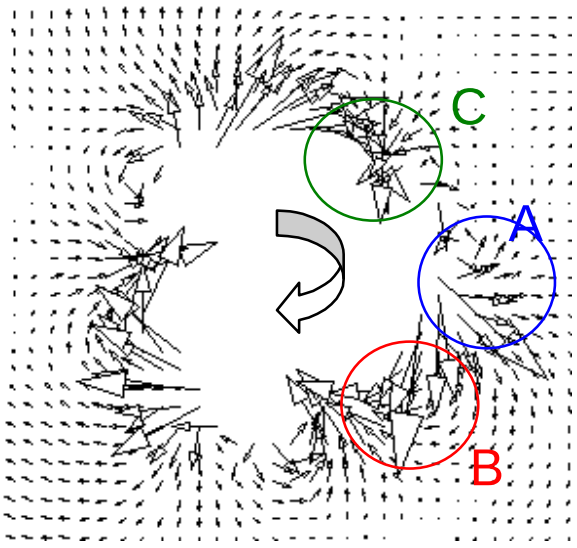

Fig. 34 Horizontal flow pattern at 0.436 s for triangular pin

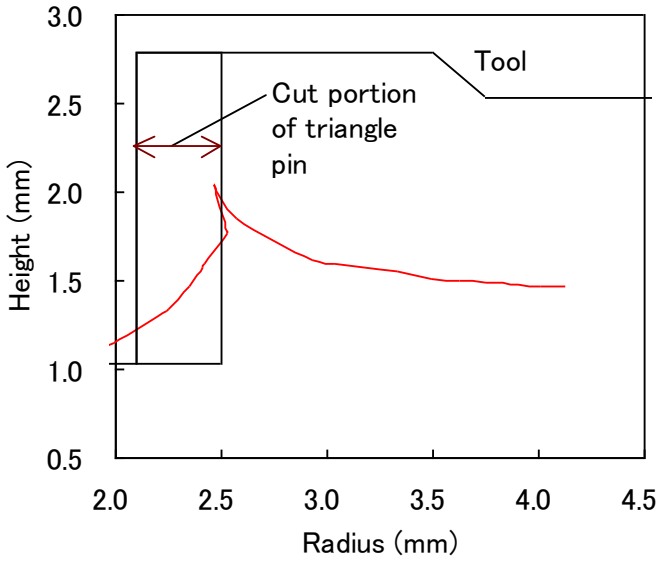

Fig. 35 Average position of particles that were originally at 1 mm from upper surface of workpiece at 0.44 s for triangular pin with concave shoulder

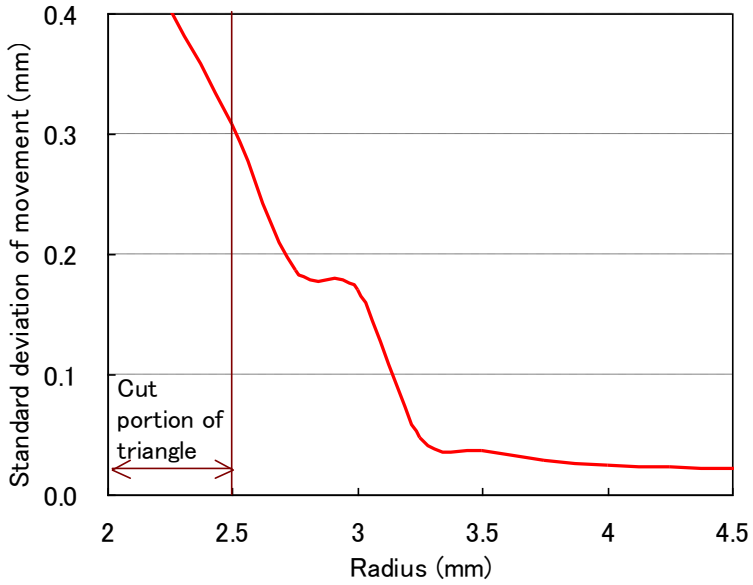

Fig. 36 Standard deviation of movement of particles at 0.44 s for triangular pin

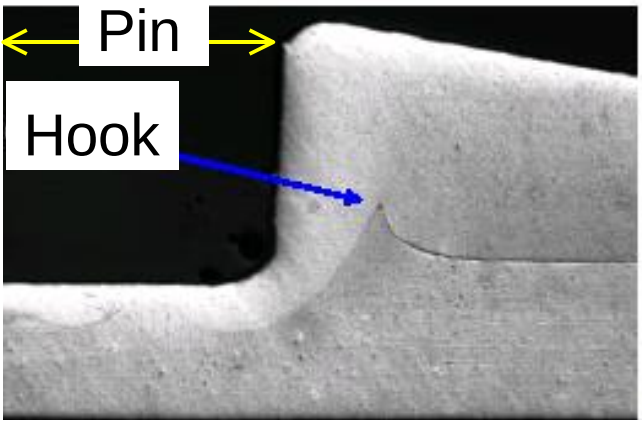

Fig. 37 Vertical cross section of FSSW weld specimen for triangular pin (Badarinarayan et al., 2009a)

SUMMARY

The effect of tool geometry on plastic flow and mixing of materials during friction stir spot welding process (FSSW) is investigated numerically using the particle method.

1. Temperature distribution is axisymmetric and the temperature below the rotating tool is 340°C at 0.44 s for the standard tool with a cylindrical pin of 5 mm diameter and pin length of 1.25 mm rotating at 1500 rpm.

2. For a cylindrical pin tool, the material flow at the pin periphery is in the upward direction. Near the shoulder, there are two flow patterns observed – beneath the shoulder, the material is pushed downward due to the force acting from the shoulder face, whereas on the shoulder periphery the material flows upward and outward due to extrusion of the material that is caused by the shoulder plunge. This material flow attributes to the formation of the 'hook' geometry. Numerical results showing the prediction on the hook formation agree well with the experimental data.

3. The triangular pin tool, due to its inherent geometry, shows enhanced material flow. This enhances flow also helps in suppressing the upward rising hook geometry (as seen in welds made with cylindrical pin). A triangular pin with a concave results in spot welds with high strength.

4. The friction stir welding tool geometry has a significant influence on the material mixing and hence eventually influences the static strength of resultant spot welds.

REFERENCES

Aratani, T., 1995, High-Speed Computing Algorithm for Molecular Dynamic Simulation, Computational Mechanics'95, Vol.2, pp.1852-1857.

Badarinarayan, H., Hunt, F., Okamoto, K., and Hirasawa, S., 2007, Study of Plunge Motion during Friction Stir Spot Welding – Temperature and Flow Pattern, Proc. 2007 The Minerals, Metals & Materials Society Annual Meeting.

Badarinarayan, H., Yang, Q., and Zhu, S., 2009a, Effect of Tool Geometry on Static Strength of Friction Stir Spot-welded Aluminum Alloy, International Journal of Machine Tools & Manufacture, Vol. 49, pp. 142–148.

Badarinarayan, H., Shi, Y., Li, X., and Okamoto, K., 2009b, Effect of Tool Geometry on Hook Formation and Static Strength of Friction Stir Spot-welded Aluminum 5754-O Sheet, International Journal of Machine Tools & Manufacture, Vol. 49, pp. 814–823.

Chao, Y.J., and Qi, X., 1998, Thermal and Thermo-Mechanical Modeling of friction Stir welding od Aluminum Alloy 6061-T6, J. of Materials Processing & Manufacturing Science, Vol. 7, No.10, pp. 215-233.

Chikazawa, S., and Koshizuka, S., 2001, A Particle Method for Elastic and Visco-Plastic Structures and Fluid-Structure Interactions, Computation Mechanics, Vol. 27, pp.97-106.

Colegrove, P. A., and Shercliff, H. R., 2004, Modeling the Friction Stir Welding of Aerospace Alloys, Proc. 5th International FSW Symposium.

Dörfler, S. M., 2008, Advanced modeling of friction stir welding – improved material model for aluminum alloys and modeling of different materials with different properties by using the level set method, Proc. of the COMSOL Conference 2008 Hannover.

Hirasawa, S. Okamoto, K., Hirano, S., and Tomimura, T., 2005, Combined Analysis of Plastic Deformation Flow and Temperature Distribution during Friction Stir Welding, Proc. 2005 ASME International Mechanical Engineering Congress and Exposition, IMECE2005-79328.

Hirasawa, S. Okamoto, K., Hirano, S., and Tomimura, T., 2006, Analysis of Temperature Distribution and Plastic Deformation Flow during Spot Friction Stir Welding, Proc. 13th International Heat Transfer Conference, MNF-03.

Hirasawa, S. Badarinarayan, H., Okamoto, K., Tomimura, T., Kawanami, T., and Hirano, S., 2009, Analysis of Temperature and Plastic Flow during Friction Stir Spot Welding using Particle Method, J. of Thermal Science and Technology JSME, Vol. 4, No. 2, pp. 260-271.

Khandkar, M. Z. H. and Khan, J. A., 2003, Predicting Residual Thermal Stresses in Friction Stir Welding, Proc. 2003 ASME International Mechanical Engineering Congress and Exposition, IMECE2003-55048.

Kondo, M., Koshizuka, S., and Suzuki, Y., 2006, Application of Simplectic Scheme to Three-Dimensional Elastic Analysis using MPS Method, Trans. JSME, Vol. 72, No. 716, pp. 425-431 (in Japanese).

Langerman, M., and Kvalvik, E., 2003, Modeling Plasticised Aluminum Flow and Temperature Fields During Friction Stir Welding, Proc. 6th ASME-JSME Thermal Engineering Joint Conference, TED-AJ03-133.

McCune, R. W., Ou, H. Armstrong, G., and Price, M., 2004, Modeling Friction Stir Welding with the Finite Element Method, A comparative Study, Proc. 5th International FSW Symposium.

Rajamanickam, N., Balusamy, V., Madhusudhann, Reddy, G., and Natarajan, K., 2009, Effect of Process Parameters on Thermal History and Mechanical Properties of Friction Stir Welds, Materials and Design, Vol. 30, No. 7, pp. 2726-2731.

Schmidt, H., and Hattel, J., 2005, A Local Model for the Thermomechanical Condition in Friction Stir Welding, Modelling and Simulation in Materials Science and Engineering, Vol. 13, pp. 77-93.

Tomimura, T., Okita, K., and Hirasawa, S., 2006, Experimental Evaluation of Apparent Dynamic Coefficient of Friction between Rotating Rod and Metal Plate, Proc. 2006 Materials Science & Technology.

Zahedul, M., Khandkar, H., Khan, J. A., Reynolds, A. P., and Sutton, M. A., 2006, Predicting Residual Thermal Stresses in Friction Stir Welded Metals, Journal of Materials Processing Technology, Vol. 174, pp. 195-203.

Zhang, Z., and Zhang, H. W., 2008, Numerical Studies on Controlling of Process Parameters in Friction Stir Welding, Journal of Materials Processing Technology, 209, pp. 241–270.

Zhang, Z., and Zhang, H.W., 2009, Numerical Studies on the Effect of Transverse Speed in Friction Stir Welding, Materials and Design, 30, pp. 900–907.